Vietnam Journal of Earth Sciences, 47(1), 136–156, https://doi.org/ 10.15625/2615-9783/22194

Vietnam Journal of Earth Sciences

https://vjs.ac.vn/index.php/jse

Drought prediction across Vietnam using a hybrid approach

Dao Nguyen Quynh Hoa*, Pham Quang Nam, Phan Van Tan

VNU University of Science (HUS), Vietnam National University, Hanoi (VNU)

Received 04 September 2024; Received in revised form 16 November 2024; Accepted 08 January 2025

ABSTRACT

Drought is one of the most pervasive and complex natural hazards, significantly impacting ecosystems, agriculture, and communities, particularly in Vietnam. The study constructed a hybrid model to explore the sensitivity of drought forecast over Vietnam, utilizing bias-corrected precipitation and temperature data from regional climate models, RegCM, and clWRF. The resulting 6-month scale Standardized Precipitation Evapotranspiration Index (SPEI-6), is then processed through two different multi-model ensemble approaches: a simple averaging method (ENS) and a more complex artificial neural network (CTL), forming the basis of our two experimental setups. CTL consistently outperformed ENS, demonstrating more substantial drought-predictive skills. CTL effectively captured the spatio-temporal distribution of SPEI-6, showing high accuracy at a 1-month lead time. Its performance is promising, particularly in regions with complex climate patterns like the Central of Vietnam (R4 and R5), though discrepancies in predicting SPEI-6 amplitudes become slightly evident at a 5-month lead time. The geographic extent analysis further supports CTL's strengths in short-term forecasting, highlighting its utility in early warning systems and immediate drought response planning. Nonetheless, the decrease in accuracy at extended lead times underscores the need for model refinement. The study contributes to the growing body of literature on ANN-based drought forecasting, emphasizing the potential and limitations of these models in the context of Vietnam.

Keywords: Drought, Seasonal Prediction, Vietnam, ANN, Hybrid approach.

1. Introduction

Droughts are among the most severe and far-reaching natural hazards, affecting numerous regions across the globe. Characterized by prolonged periods of abnormally low rainfall, droughts lead to significant water shortages that adversely affect ecosystems, agriculture, and human communities (WMO, 2006). The slow onset and the insidious nature of drought make it particularly challenging to monitor and manage. Under the global warming scenario, changes in precipitation patterns, increased evaporation rates, and more frequent extreme weather events are likely to cause more severe and prolonged droughts (Dai, 2011; Spinoni et al., 2020; Thilakarathne and Sridhar, 2017; Trenberth et al., 2014).

Drought is generally categorized into four distinct types: meteorological, agricultural, hydrological, and socio-economic droughts (Heim Jr, 2002; Vu et al., 2013). Meteorological drought is defined by a prolonged period of below-average precipitation, which can lead to water deficits in the atmosphere and surface. Hydrological

*Corresponding author, Email: hoadao@vnu.edu.vn

drought concerns precipitation shortfalls' effects on water resources, such as rivers, reservoirs, and groundwater levels. According to Wilhite and Buchanan-Smith (2005) and Guttman (1999), the delay between the onset of a meteorological drought and the development of a hydrological drought underscores the importance of early detection. Precipitation-based drought indices are often the earliest indicators of drought onset, serving as critical tools for detecting and monitoring meteorological drought conditions, thereby mitigating long-term consequences (Woldeyohannes et al., 2019). Yihdego et al. (2019) and Zargar et al. (2011) provided a comprehensive overview of over 150 drought indices developed over the years. The diversity of drought indices reflects the complex nature of drought, encompassing various factors such as precipitation, temperature, soil moisture, and vegetation health (McKee et al., 1995; Mckee et al., 1993). While validating every single index, the Standard Precipitation Evaporation Index (SPEI) (Beguería et al., 2014; Vicente-Serrano et al., 2010) has gained increasing acceptance in recent years. SPEI is derived from precipitation and evapotranspiration and is primarily used to identify meteorological and hydrological droughts. The main advantage of using SPEI as a drought index is that it is not negatively impacted by topographic variations, allowing for consistent application across diverse landscapes. Additionally, the standardization of SPEI ensures that the frequencies of extreme events are consistent across different locations and timescales, providing a reliable measure for comparing drought severity in diverse regions, as noted by Hao et al., 2018.

Climate conditions in Vietnam are influenced by Southeast Asia and Indian monsoons, resulting in distinct wet and dry seasons (Phan-Van et al., 2022; Vu et al., 2013). These climate variabilities significantly affect water availability, thus agricultural productivity, and ecosystem health across different regions of Vietnam. Previous studies have extensively documented the observed differences in drought characteristics among subregions in Vietnam, highlighting the region's vulnerability to varying drought conditions (Le et al., 2019; Phan-Van et al., 2022; Vu et al., 2013). These studies have provided valuable insights into the linkages between drought in Vietnam and large-scale drivers, land use changes, and climate variabilities.

Thus, accurate and timely drought forecasting is essential for effective water resource management, agricultural planning, and disaster mitigation in Vietnam. Traditional methods of drought prediction often rely on statistical models or physical approaches (Deo and Şahin, 2015; Hao et al., 2018; Mishra and Desai, 2005; Wang et al., 2018) that may not fully capture the complex, nonlinear relationships between climatic variables. With advances of computational technology and data availability, machine learning-based methods have emerged as a powerful tool for forecasting extreme phenomena like droughts (ASCE, 2000; Mishra and Singh, 2011). Artificial neural networks (ANNs) are well-suited to modeling the intricate interactions between meteorological variables that drive drought conditions, offering a flexible and adaptive approach to prediction (Spinoni et al., 2020). The ANN is an informative processing approach that mimics the structure and function of the brain (McCulloch and Pitts, 1943). Given sufficient data and complexity, ANNs can effectively identify nonlinear relationships between series of independent and dependent variables – inputs and outputs to the network, respectively (Hornik et al., 1990). A striking advantage of

ANNs is that the modeler does not need to fully define the intermediate relationships (i.e., physical processes) between inputs and outputs (Sudheer et al., 2003). Various architectures of ANNs have been investigated globally in drought prediction and assessment, including feedforward networks (Ali et al., 2017; Mishra and Desai, 2006; Santos et al., 2009), recurrent neural networks (Le et al., 2017; Sardar et al., 2021; Shobha et al., 2023), convolutional neural networks (Sardar et al., 2021; Zhang et al., 2024), to capture the complex interactions between climate variables that influence drought conditions. Nonetheless, the contribution of physically based climate models to drought forecasting, spanning from intra-seasonal to seasonal scales, is undeniable. These models provide essential support by offering detailed and scientifically grounded insights into climatic trends and anomalies, though their reliability is still relatively low (Alley et al., 2019; Becker et al., 2014). Over the years, a broad spectrum of regional climate models has been developed globally (Watanabe et al., 2010). To benefit from the strengths of these diverse models and address the limitations inherent in individual dynamical models - such as resolution and parameterization - there has been an increasing trend toward combining multiple models and their forecasts (Rayhan and Afroz, 2024). This approach enhances the robustness and accuracy of predictions by integrating the unique capabilities of each model. Hybrid models - the combination of both physical and statistical-based models - have gained attraction in drought forecasting over recent decades (Adnan et al., 2021; AghaKouchak et al., 2022; Madadgar and Moradkhani, 2014; Wu et al., 2022; Zhang et al., 2015). With the advancements highlighted in their studies, they underscore the need for ongoing research in developing new strategies incorporating hybrid models in drought prediction.

The abovementioned studies have inspired us to contribute to the growing body of literature on applying hybrid models incorporating ANN techniques in drought forecasts. Building upon this foundation, the primary objective of this study is to develop a novel integration of a hybrid model and examine how the inclusion of ANN impacts the predictability of drought events over the mainland of Vietnam. We combine linear and nonlinear algorithms within a workflow centered on the SPEI at a 6-month scale optimized for drought forecasting in Vietnam. The rationale behind using an ensemble of dynamic models that integrates nonlinear and linear statistical methods is to leverage the unique strengths of each model type, enabling us to capture diverse patterns in the data. By investigating these various hybrid configurations, we aim to enhance our understanding of the potential and limitations of these models in accurately forecasting drought conditions in this region. Despite advances in machine learning, limited studies have explored the application of ANN for drought prediction across multiple subprocesses in this basin. To address this gap, this study proposes a novel approach that optimally tunes and integrates ANN models in a systematic framework for improved drought forecasting. The paper is organized as follows. Section 2 describes the data, ANN-based experimental designs, and verification metrics of drought conditions in Vietnam. The verification and comparison between the experiments are then presented in Section 3. Finally, the conclusion is given in Section 4.

2. Data and methods

2.1. Study area

The study area covered in this study encompasses the entire mainland of Vietnam.

As shown in Fig. 1, Vietnam is located in the South East Asia. The area is generally classified into 7 subregions in distinctive climate patterns, topography conditions, and latitudinal extents (Phan-Van et al., 2009; Van Khiem et al., 2014). Due to diverse geographical locations and monsoon conditions, the dry season period varies significantly among subregions: R1 (Northwest), R2 (Northeast), R3 (Red River Delta), R4 (Northcentral), R5 (Southcentral), R6 (Central highland), and R7 (South).

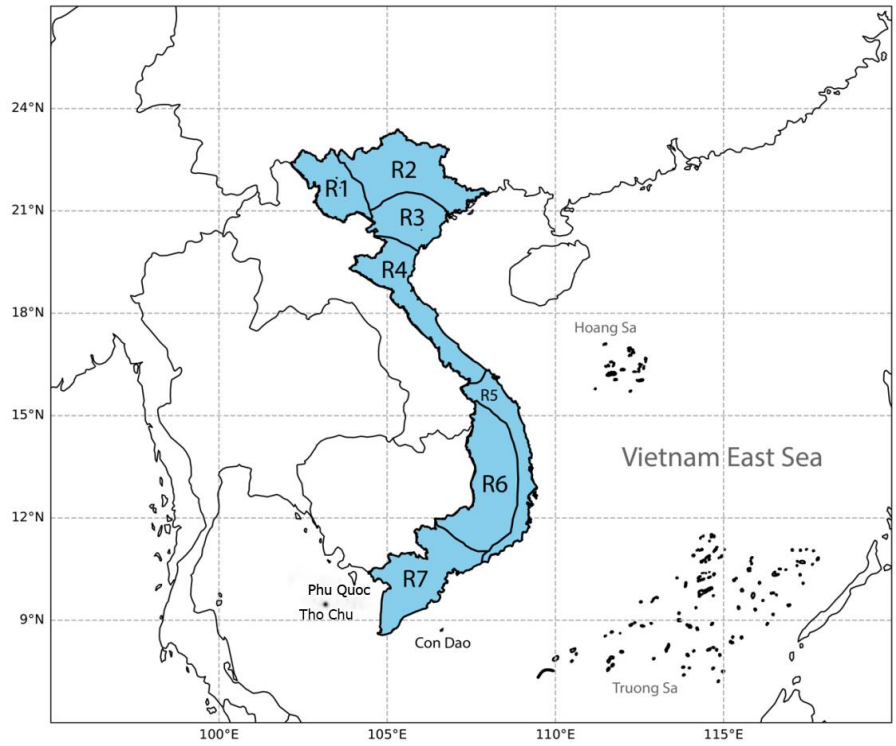

Figure 1. The highlighted study area (blue) divides in 7 subregions (from R1 to R7)

2.2. Standard Evapotranspiration Precipitation Index and Drought Characteristics

To investigate drought conditions, we utilized the Standardized Evapotranspiration Precipitation Index over 6 months (SPEI-6). The general SPEI is widely used for quantifying water deficits at various time scales (Beguería et al., 2014; Vicente-Serrano et al., 2010).

Accounting for the spatio-temporal variations in water deficits, the algorithm transforms the time series of climatic water balance ($D_i = Pr_i - ET_i$) into the Log-logistic probability distribution with zero mean and one standard deviation. Pr_i is precipitation and ET_i is evapotranspiration aggregated at i-th time scales. Currently, the calculation benchmark of potential evapotranspiration (PET) refers to the Thornthwaite method, using surface temperature (Thornthwaite, 1948). To be more specific, readers are encouraged to refer to previous studies for detailed mathematical explanations of SPEI and its various modifications (Habeeb et al., 2023; Zarei and Moghimi, 2019). The three commonly used timescales are 3-month, 6-month, and 12-month. While the SPEI-3 corresponds to short-term agricultural drought, the 12-month timescale reflects the

characteristics of year-round drought variability (Steinemann et al., 2005; Tan et al., 2015). Given the strong seasonal variability of water deficits in dry - wet seasons and monsoon conditions in Vietnam, the 6-month is considered the more appropriate indicator (Nguyen et al., 2014; Phan et al., 2014; Phan and Ngo-Duc, 2009; Vu et al., 2015; Zhang et al., 2002). Therefore, we use SPEI-6 as the key metric to quantify drought characteristics, capturing the water cycle's response to precipitation anomalies.

A drought event in the context of SPEI-6 is a period characterized by dryness whose SPEI-6 falls below a pre-defined threshold (Table 1). A negative SPEI indicates drier periods, giving an alert for a drought event. The study will mainly focus on moderate or severe droughts, corresponding to SPEI-6 values less than or equal to -1.

Table 1. Drought categories by SPEI-6 (Beguería et al., 2014; Vicente-Serrano et al., 2010)

SPEI	Drought category
0 > SPEI > -1	Mild drought
-1 ≥ SPEI ≥ -1.5	Moderate drought
-1.5 ≥ SPEI > -2	Severe drought
SPEI ≤ -2	Extreme drought

2.3. Data

This study calculated drought indices using the following datasets: (1) observed gridded monthly precipitation/temperature data, and (2) monthly precipitation/temperature data predicted by dynamical models, following bias correction.

Gridded monthly precipitation data (VnGP) with a resolution of 0.25 degrees were derived from daily precipitation measurements collected from a network of meteorological stations across Vietnam for the period 1980-2020 (Nguyen-Xuan et al., 2016; Tran-Anh et al., 2022). These data were used to calculate a drought index, which assisted in identifying observed drought events to verify the performance of the model predictions.

Monthly predicted precipitation data were derived as follows: First, forecast data from the NCEP CFSv2 (Saha et al., 2014), with a resolution of 1.0 degrees and a lead time of 6 months, were downscaled to a 20 km resolution using two Regional Climate Models (RCMs), RegCM and clWRF. Downscaling products from the RCMs, including precipitation, temperature, geopotential height, wind, humidity, and other variables, were then remapped to a 0.25-degree resolution and used to adjust the model precipitation by using gridded precipitation data as a reference.

The downscaled forecast datasets were subsequently bias-corrected in three methods: (1) adjustments based on the differences between the model and observed climatology (Cli); (2) Artificial Neural Network (ANN1), and (3) Multiple Linear Regression (MLR). We divided the observed and forecast data into training and validation sets to achieve this. The training was performed in two steps: the first used data from 1982 to 2011 for training, and the second employed data from 2011 to 2020 for validation. The iterative process involved adjusting various parameter settings and input variables until the model's performance stabilized.

2.4. Hybrid model settings and experimental design

Figure 2 illustrates the flowchart of the hybrid model used for calculating SPEI on a 6-month scale, outlining the steps involved in all experiments (highlighted in yellow boxes).

As noted above, the calculation of SPEI requires bias-corrected precipitation and surface temperature from RCMs, specifically clWRF and RegCM4. The bias-correction

section highlights three distinct approaches: Cli, ANN1, and MLR.

The first method, labeled Cli, involves adjustments based on the differences between model-generated and observed climatology. This straightforward method relies on aligning the model data with observed historical records. Specifically, for precipitation R and temperature T, we have:

$$R_{Cli} = R_{mod} * \delta R;\ \delta R = \overline{R_{obs}}/\overline{R_{mod}}$$
$$T_{Cli} = T_{mod} + \Delta T;\ \Delta T = \overline{T_{obs}} - \overline{T_{mod}}$$

Subscript "*mod*" denotes individual model output, and "*obs*" denotes observation, while the overline represents a temporal average of the variable from 1982 to 2011. ANN1 and MLR are nonlinear and linear statistical approaches to perform bias correction of model outputs. In the context of bias correction, the artificial neural network adopted at ANN1 uses the input variables X (X could be R_{mod}, T_{mod}, and other model outputs including daily minimum and maximum temperatures, geopotential height at levels 850 hPa and 500 hPa, outgoing longwave radiation OLR, specific humidity at 2m, relative humidity at 2m, sea level pressure, zonal wind at 200 hPa and 850 hPa, and vertical velocity at 700 hPa) to learn and predict the corrections needed (Y) to align these variables more closely with observation. Whereas MLR assumes a linear relationship between the input and the correction factors by adjusting the slope and intercepts of the linear model:

$$Y = F(X)$$

The function F(X) could be either nonlinear (ANN) or linear (MLR). Our MLR offers the Ordinary Least Squares method to estimate the coefficients α and intercept β to solve the function $Y = \alpha X + \beta$. Details of ANN1 shall be discussed further in the following section. It is important to note that all inputs are normalized to avoid differences in units between variables.

Afterward, the output monthly rainfall and temperature recreated from each bias-corrected model serve as a benchmark for deriving SPEI-6 for subsequent drought analyses.

At each bias-corrected model output, the SPEI-6 index was calculated as input toward the multi-model ensemble approach (illustrated in Fig. 2b). The potential evapotranspiration (PET), a key component in calculating SPEI, was estimated using the Thornthwaite method based on surface temperature (Thornthwaite, 1948). We aggregated bias-corrected R and PET over 6 consecutive months at each lead time to compute SPEI-6. Combining SPEI-6 outputs from the 6 models corrected through Cli, ANN1, and MLR in the 2 RCMs, the ensemble method aims to mitigate the inherent uncertainties and biases in individual models.

We conducted two experiments to combine the ensemble members' outputs: one using a simple ensemble mean approach (ENS) and the other (CTL) employing the artificial neural network. ENS aggregates outputs of individual models by averaging SPEI-6. On the other hand, CTL utilizes a more complex neural network structure (ANN2) to combine the ensemble members, aiming to capture nonlinear relationships and interactions between inputs that the ensemble mean might overlook. These two methods were applied to integrate the bias-corrected outputs, offering different perspectives on improving drought prediction accuracy through hybrid modeling. The next section will describe the neural network architectures adopted in ANN1 and ANN2.

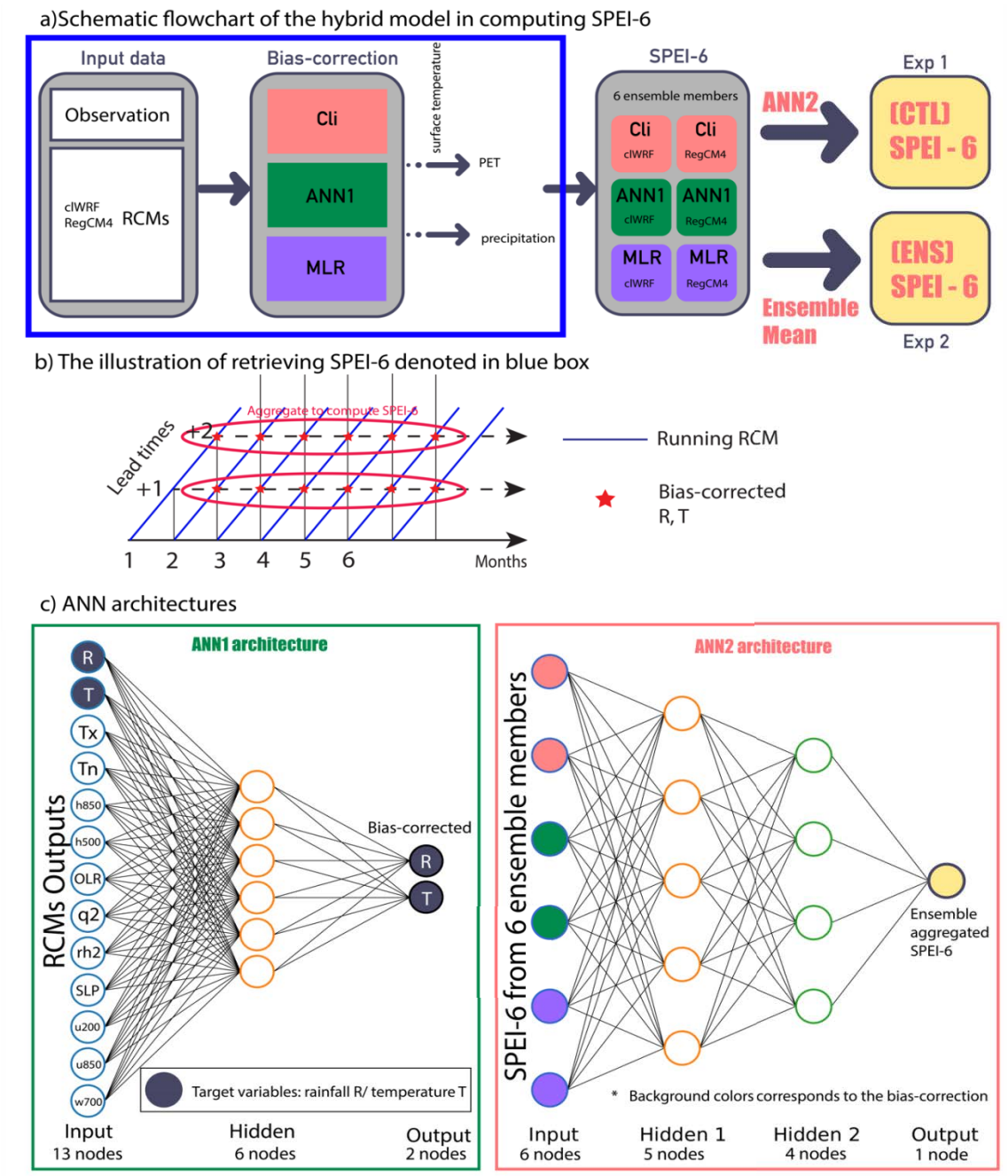

Figure 2. a-b) Schematic diagram of the hybrid model and experimental design (yellow boxes) and c) the Artificial Neural Network architectures designated in the drought forecasting procedure. In ANN1, the input nodes include rainfall R_{mod}, temperature T_{mod}, and various model outputs (see text for further descriptions); and the output nodes include bias-corrected R and T. In ANN2, the input layer includes SPEI-6 from the 6 ensemble members (background colors corresponds to the bias-correction), and the output includes ensemble aggregated SPEI-6 through neural network

2.5. Artificial Neural Network (ANN)

Each network structure (Fig. 2c) consists of neurons organized into interconnected groups known as layers. Every ANN includes a sequence of an input layer, a hidden layer(s), and an output layer. We design two subprocesses using a feedforward neural network for drought forecasting with adaptive and distinct architectures, namely ANN1 and ANN2. The major differences between ANN1 and ANN2 include (1) multilayer perceptron architecture and (2) numerical solution for gradient descent. They are explicitly configured on their roles in the hybrid model, following specific rules.

2.5.1. Multilayer Perceptron Architecture

In this term, the number of hidden layers varies between the two architectures. In ANN1, each output layer comprises 2 nodes, including rainfall and temperature. The input layer contains 13 nodes for standardized model outputs: rainfall R, temperature T, minimum and maximum temperature (Tx and Tn), geopotential height at 850 and 500 hPa (h850 and h500), outgoing longwave radiation OLR, specific humidity at 2 m (q2), relative humidity (rh2), sea level pressure SLP, zonal winds at 200 hPa (u200) and 850 hPa (u850), and vertical velocity at 700 hPa (w700). The architecture of the ANN1 is based on the feedforward multilayer perceptron with only one hidden layer, which has already been applied to drought forecast (Belayneh et al., 2014; Kim and Valdés Juan, 2003; Morid et al., 2007).

Nevertheless, recent studies (Mezard and Nadal, 1999; Schmidt and Overhoff, 2022) show that the increase of hidden layers and neurons can enable the network to learn more complex representations of input data, thereby capturing intricate patterns that a simple feedforward multilayer perceptron might miss. We construct ANN2 with a more complicated architecture than ANN1, including 2 hidden layers. Each hidden layer contains a total of 5 and 4 nodes, respectively. The input layers include SPEI-6 from bias-corrected 6 ensemble members and the output layer consists of a single node representing the post-processed SPEI-6 (see the right panel of Fig. 2b). The design aims to integrate the information from a multi-model ensemble into a unified forecast in a nonlinear perspective to compensate for the lost efficiency when adapting the 6 ensemble models (Kůrková, 1992).

In both ANN1 and ANN2, the number of nodes in each hidden layer may vary without a fixed rule. However, as the input nodes should reduce to the number of output nodes, they are chosen to lessen gradually and between the sizes of the input and output layers (Heaton, 2008).

2.5.2. Numerical Solution for Gradient Descent

Gradient descent is an optimization algorithm commonly used to find optimal weights of a neural network by minimizing the cost function $J(\theta)$ during training. A stochastic gradient descent starts with putting random weights $\theta = \theta_0$. After that, the weights are adjusted in the opposite direction of the gradient to reduce the loss. The size of the adjustment is determined by the learning rate η. At each iteration, new weights are updated by Eq. 1 until the loss function converges to a minimum:

$$\theta_i = \theta_{i-1} - \eta \cdot \nabla_\theta J(\theta) \quad (1)$$

ANN2 adopts a simple gradient descent solver with the steps above, which is straightforward to implement and consumes less memory. This simple algorithm often results in slower convergence and may quickly get stuck in local minima. The addition of momentum v works as a solution for this problem (Eq. 2):

$$v_i = \alpha \cdot v_{i-1} + \eta \cdot \nabla_\theta J(\theta)$$
$$\theta_i = \theta_{i-1} - v_i \quad (2)$$

with α is the momentum factor. In ANN2, we choose $\alpha = 0.7$.

Apart from these differences, ANN1 and ANN2 share several similar features in their training processes. Both networks are trained over 1000 epochs; the activation function is sigmoid. Additionally, a consistent learning rate of 0.02 was applied in both cases with an early stopping technique to halt training early if the validation loss began to increase. We adopted a random initialization method, randomly initializing the weights and biases from the normal distribution to ensure stochastic starting points for the parameters. These configurations were calibrated carefully and trained multiple times to avoid overfitting and sensitivity to initial parameters. These shared parameters ensure a fair comparison between the two architectures, focusing the evaluation on the impact of network complexity on drought predictive performance.

2.6. Verification metrics

Correlation coefficients

To evaluate the accuracy and reliability of drought event prediction made by the SPEI-6, categorical skill scores are used as statistical measures. The scores compare the predicted drought month against observed SPEI-6 to determine how accurately the model forecasts dry and wet conditions in time and space.

Categorical skill scores

The drought occurrence is calculated based on SPEI-6 values falling below a specific threshold (see Table 1). We focus on the onset of moderate drought events (SPEI-6 < -1) and verify the model performance in terms of a number of yes/no events as in the contingency table (Table 2).

Table 2. Contingency table to verify moderate or severe drought events by SPEI-6 < -1

Drought event forecast	Drought event observed		
	Yes	No	Marginal total
Yes	a	b	a + b
No	c	d	c +d
Marginal total	a + c	b + d	N

- Accuracy (or Proportion Correct) measures how often the model's predictions match the actual observation over time. It represents the Proportion of correct predictions relative to the total number of predictions made (see Eq. 1).

$$Accuracy = \frac{a+d}{N} \text{ (Eq. 1)}$$

- Probability of Detection (POD) measures the Proportion of observed moderate drought events (SPEI-6 below -1) that the model correctly predicted. POD ranges from 0 to 1, where 1 indicates perfect detection of all drought events.

$$POD = \frac{a}{a+c} \text{ (Eq. 2)}$$

- Heidke skill score (HSS) measures the accuracy of the model's prediction relative to random chance, accounting for hits, misses, and false alarms. HSS ranges from -∞ to 1, where 1 indicates perfect accuracy, and 0 indicates no skill compared to random chance.

$$HSS = \frac{2\times(a\times d-b\times c)}{(a+c)\times(c+d)+(a+b)\times(b\times c)} \text{ (Eq. 3)}$$

- Threat score (TS) evaluates how well the model predicts the occurrence of drought events (both hits and misses) and penalizes for false alarms. TS ranges from 0 to 1, with 1 indicating perfect accuracy.

$$TS = \frac{a}{a+b+c} \text{ (Eq. 4)}$$

3. Results and discussion

3.1. Prediction skill

This section of the paper deals with the performance evaluation of the proposed frameworks. To provide a brief overview of how well the forecasted SPEI-6 aligns with observation, Fig. 3 presents the correlation coefficients between predicted and observed datasets from 1983 to 2020 for the 2 experiments. The correlations generally exhibit minor variations across different regions and lead times. In CTL, the correlation coefficients are relatively high across most regions of Vietnam, with values primarily ranging from 0.75 to 0.95. Additionally, the correlations

seem to decrease with extending lead times for most subregions, notably observed in R3, though still generally high even at a 6-month lead time. As for R5, the maxima of correlations peak at 4 and 5-month lead times, concentrating to the north of the area. The peaks of high correlations are found mainly in R1, and R5-R7, indicating a good alignment with the trend in observed SPEI-6 in these subregions.

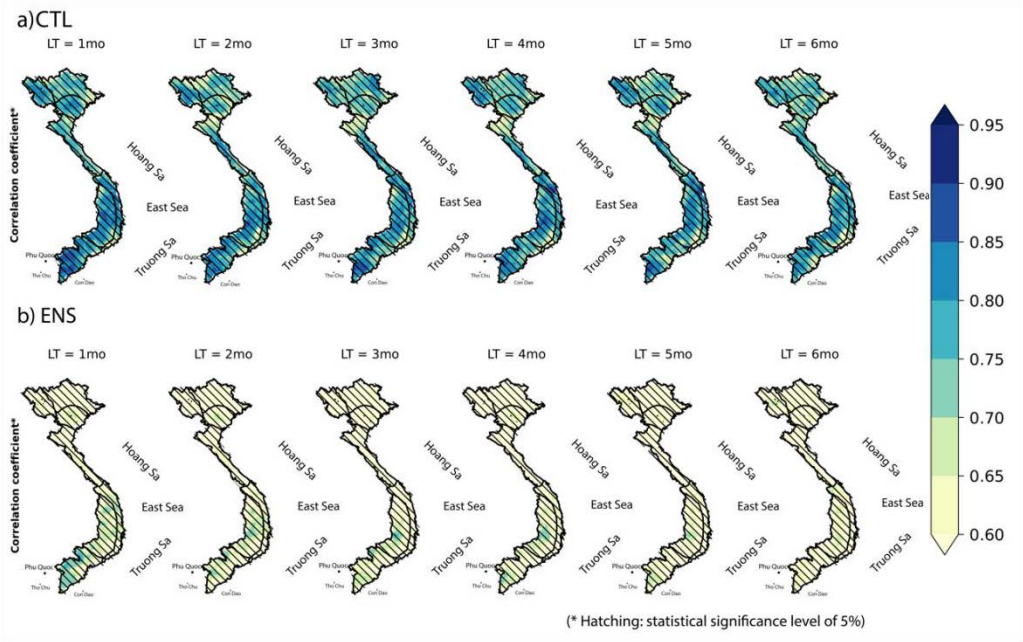

Figure 3. The spatial distribution of correlation coefficients between SPEI-6 ensemble means and observations, estimated from CTL (a) and ENS (b). The correlations are examined over lead times ranging from 1 to 6 months during 1983–2020

The correlation coefficients at ENS are lower than the CTL experiment (Fig. 3b), with values mostly ranging from 0.6 to 0.75; the highest values do not exceed 0.8. The decrease in correlation with increasing lead time at ENS is more noticeable. However, especially in the earlier lead times (LT = 1mo to 3mo), southern regions (including R5-6) tend to show slightly higher correlations than the northern regions. As the lead time increases, this distinction becomes less pronounced, exhibiting weak correlations overall. As noted in previous studies, these subregions are particularly vulnerable to severe drought (Le et al., 2019).

As classified in Table 1, different threshold values cut off dry or wet periods. When correlations coupled with the accuracy index (Fig. 4), the results demonstrate an overall promising predictability of the neural network inclusion in the ensemble (CTL). The predicted accuracy for drought and non-drought events exceeds 0.8 at every lead time across the entire domain, with particularly high accuracy in the southern part of Vietnam (R6-R7). At a 1-month lead time, most areas show accuracy levels above 0.85. However, by the 6-month lead time, some subregions, particularly in the north (R1-5), see accuracy reductions to around 0.78 to 0.82. Among the two models, CTL has performed better than ENS across all lead times, where accuracy exceeds 0.86 in most of the subregions. CTL also demonstrates less degradation in drought forecast at longer lead times, with ENS predictability decreasing more significantly, from around 0.82 to as low as 0.7.

To provide a more detailed comparison between CTL and ENS, we adopt further categorical indices to evaluate the neural network's performance in predicting moderate drought occurrences on a monthly scale, including POD, HSS, and TS (Figs. 5 and 6).

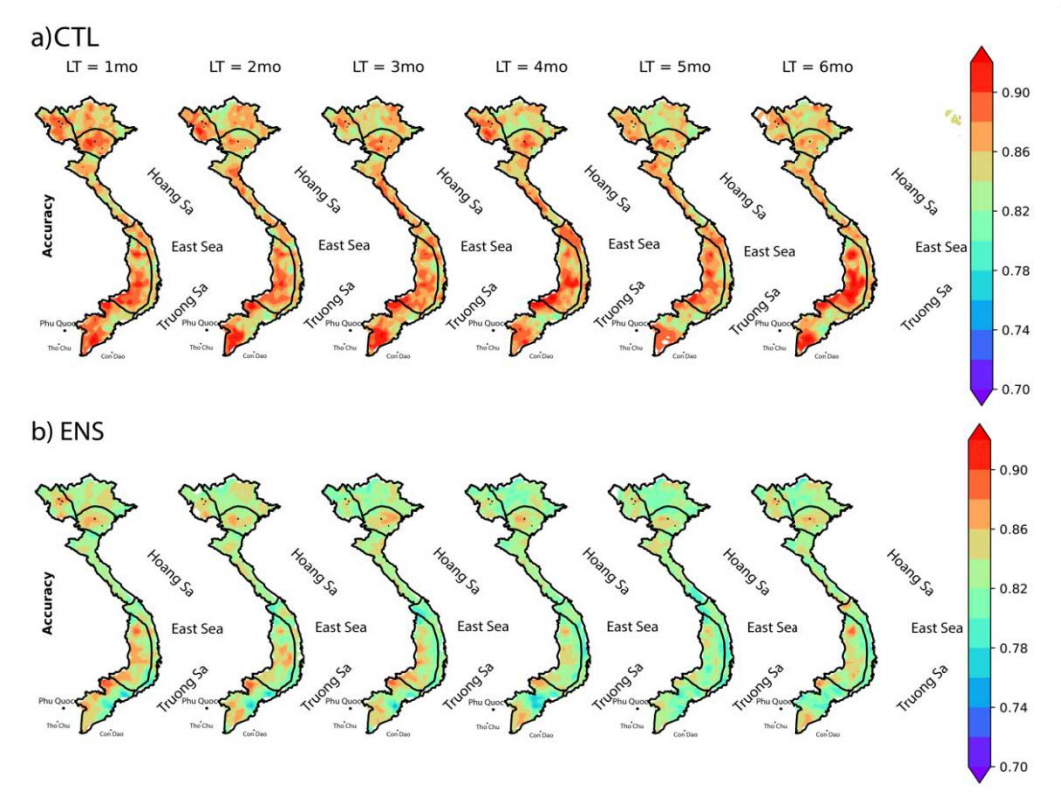

Figure 4. Accuracy index of (moderate and above) Drought Events categorized by SPEI-6 below -0.5

By CTL, both POD and HSS are significantly high in R1, R6-7 and tend to decrease as lead time increases (Fig. 5). In contrast, the predictive scores of the remaining subregions exhibit sparse and unstable minima, below 0.4 in POD and 0.5 in HSS, in their spatial distribution. As TS is lower than POD at every lead time (Fig. 3c), the model is good at detecting actual drought events despite incorrectly predicting some false alarms. Although the forecasted SPEI-6 at some points in the Central area (R4 - R5) is relatively following the observation (high correlation in Fig. 2a), the categorical skill scores indicate less skill in accurately classifying drought events.

Although there is minor variation in correlation coefficients and accuracy index (Figs. 3-4), drought categorical indices clearly show that CTL excels ENS in terms of moderate or more severe droughts (Fig. 5 vs. Fig. 6). Overall, CTL outperforms in predicting drought events in every subregion, where the accuracy, POD, HSS, and TS are relatively higher, indicating good predictability and fewer false alarms. The northern part of Vietnam (R1-4) shows lower scores, including weaker drought predictability. In these subregions, high PODs (above 0.8) are noticeable at shorter lead times (1-3 months) but decline to lower values (around 0.6) at longer lead times (especially at 5 months) meanwhile, the prediction skills of ENS decline in extended

lead times, particularly in R6-7. ENS shows less spatial consistency than CTL, with higher scores scattered and less prevalent. The drop-off at longer lead times in the southern region (R5-7) is also more pronounced. R3's drought events are better predicted at 1-month and 3-month scales, similarly in CTL and ENS.

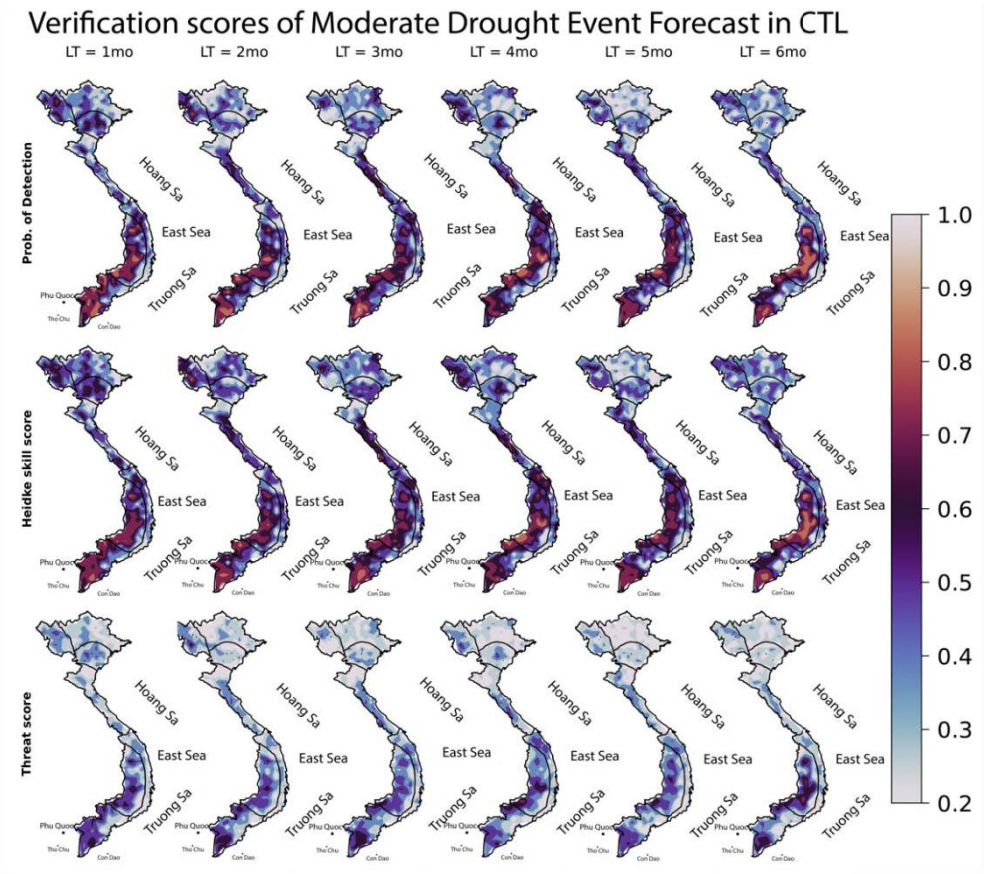

Figure 5. Categorical verifications (POD, HSS, TS; see text for details) for Moderate Drought Event Forecast categorized using SPEI-6 calculation in CTL

The above discussion reflects the spatial variability depicting the accuracy of forecasted drought events. A possible reason for the spatial variation of predicted SPEI-6 over Vietnam is that SPEI-6 serves as an integrated dry-wet classification but indirectly reflects fluctuations in predicted rainfall and temperature. These prediction skills highly depend on each subregion's regional climate variability and topographic factors. The spatial variability of SPEI-6 aligns well with the verification map of NCEP CFSv2-predicted rainfall made by Phan-Van et al. (2018). They stated the rainfall patterns are predicted more accurately in the southern regions and that the local rainfall band in Central Vietnam (R4-5) shows good agreement between model and observation, which is also visible in our predicted SPEI-6. Since NCEP CFSv2 serves as our initial and boundary conditions, their findings are directly relevant to our study. As lead time increases, forecast uncertainty typically rises (Lorenz, 1963), affecting drought predictability. Early lead times may allow the hybrid model to rely on the initial conditions

and monthly trends, often resulting in higher accuracy. This principle is reflected in our study, as shown by the model's performance over different lead times.

Understanding how effectively the neural network represents drought conditions hinges on analyzing the time series of the index values and the corresponding drought categories. Since it's impractical to show the variation of SPEI-6 for every experiment and lead times, we concentrate on the simulation results of CTL due to its superior performance at 1-month and 5-month ahead in the next section.

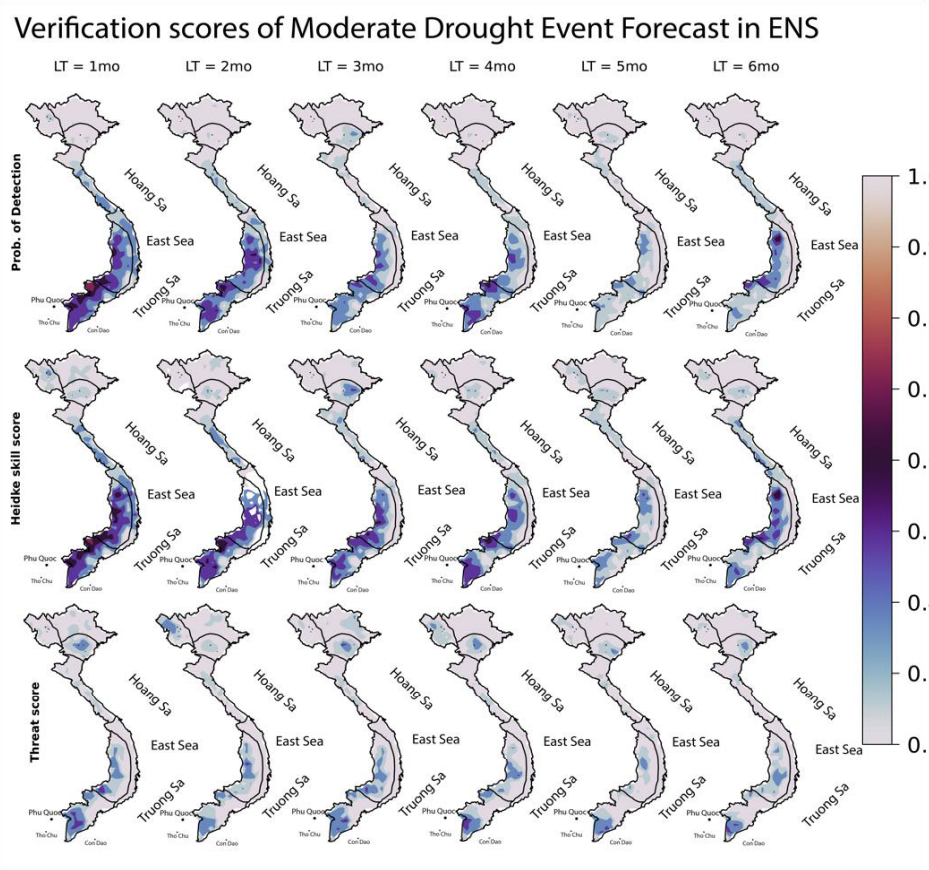

Figure 6. Categorical verifications (POD, HSS, TS) for Moderate Drought Event Forecast categorized using SPEI-6 calculation in ENS

3.2. SPEI-6 values

Figures 7-8 illustrate the temporal variation of the regional mean SPEI-6 index at different forecast lead times in both observations and CTL. Overall, the model effectively captures the evolution of the SPEI-6 index across all subregions and lead times. Although there are some minor discrepancies, the model generally simulates the index amplitude well in most subregions compared to observations. However, the difference in amplitude between neural network simulations and observations becomes more pronounced in subregions R2 and R5, where the model appears to lag slightly behind the observed data in capturing the onset or end of drought periods. The amplitude of fluctuations in SPEI-6 varies across regions. For example, the model tends to slightly underestimate the peaks of SPEI-6 values at R4 and R6,

suggesting a mismatch in classifying drought events between these two datasets. This is also a minor limitation of the hybrid model in capturing the intensity of extreme drought events due to the smoothing effects in downscaling and bias-correction processes.

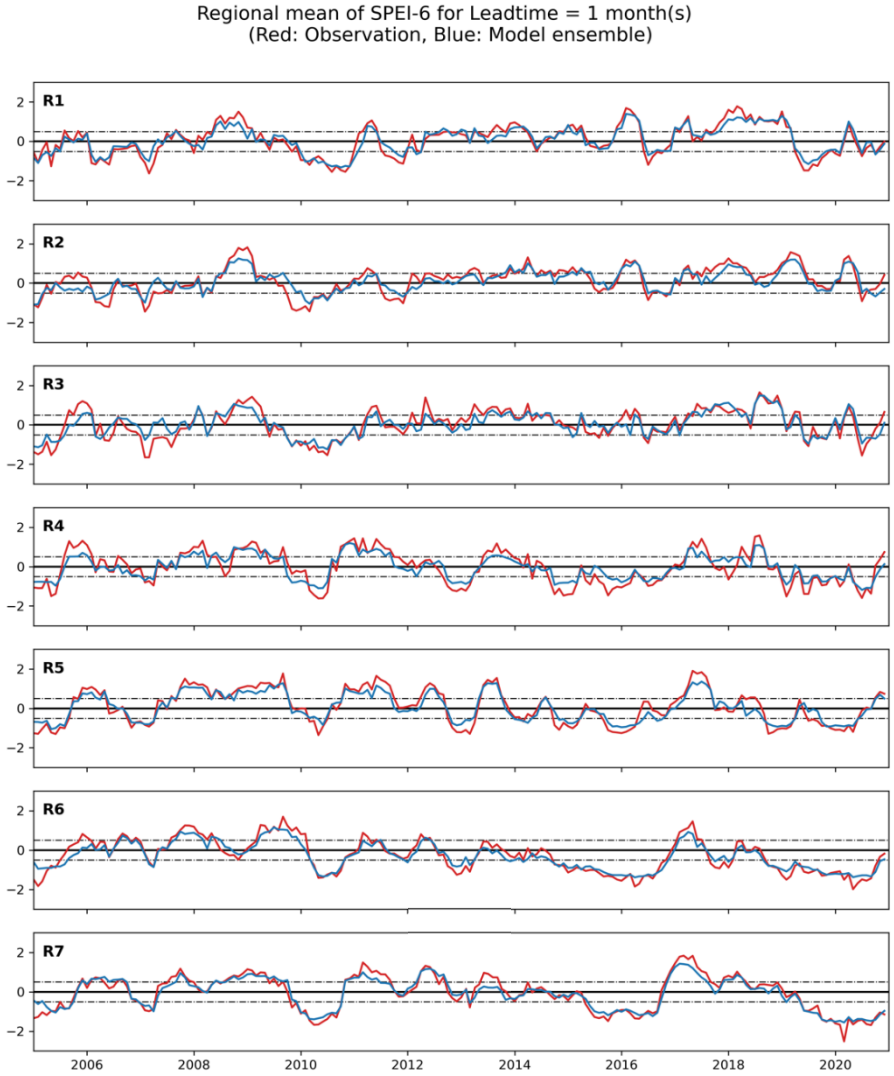

Figure 7. Evolution of the regional mean SPEI-6 for 1-month forecast by CTL model at different subregions in Vietnam. Dashed lines remark SPEI-6 at specific thresholds at -0.5 and 0.5

The 1-month lead time simulations (Fig. 7) demonstrate the highest consistency with observations, while the model's performance declines with longer lead time forecasts. The model generally captures the overall trend and variability of the observed SPEI-6, particularly in subregions R1, R3, and R7. Both the observations and model highlight moderate drought events in certain years and regions, such as around 2008–2011 and 2019–2020. A prominent feature is that the subregions display distinct forecasted SPEI-6 patterns. For instance, R3 and R5 experience more extreme fluctuations, aligning with observations. It is opposed to R4-7, which shows relatively stable conditions. These

regions might experience more frequent and prolonged drought conditions, with droughts occurring 3-4 times per decade and lasting up to 4-6 months in some cases. From 2019 to 2020, the observed SPEI dips below -2.0, indicating severe drought, whereas the model shows a milder drought with SPEI of -1.5 (R6) and 1.8 (R7).

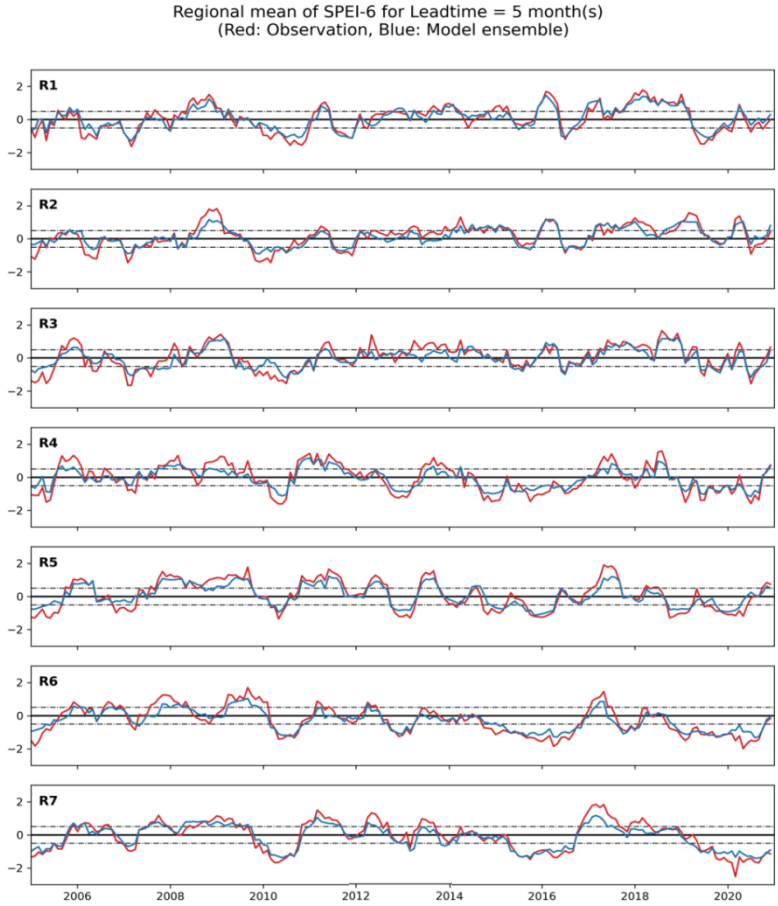

Figure 8. Evolution of the regional mean SPEI-6 for 1-month forecast by ENS model at different subregions in Vietnam. Dashed lines remark SPEI-6 at specific thresholds at -0.5 and 0.5

The model still performs excellently at longer timescales (5-month lead time, Fig. 8), especially in subregions R1 and R7, where the model closely follows the observed trends and fluctuations corresponding to seasonal and interannual variations. In some cases, more pronounced discrepancies are presented. Remarkably, the amplitude differences become more noticeable during extreme drought events (underestimation in R2-6). The extremes in dry and wet conditions appear more moderate in the model ensemble at the 5-month lead time compared to the 1-month lead time. This smoothing effect in longer lead times could be due to the model averaging more extreme variations over the extended period. Also, the model seems to lag slightly behind observed data, particularly in sharp transition periods from wet to dry conditions or vice versa. At R5, R6, and R7, the model's performance is still good, though some minor deviations in amplitude are

observed, particularly in the later years (post-2018). This suggests a decline in predictive accuracy compared to 1-month timescale.

3.3. Spatial distribution of droughts

Accurately predicting the geographical extent of drought is crucial for effective drought management. This section continues examining the performance of CTL model in forecasting the spatial distribution of moderate droughts across the seven subregions (R1-R7), focusing on the comparison between short-term (1-month lead time) and longer-term (5-month lead time) forecasts. The verification spans 2005 to 2020. The red areas represent the observed extent of drought, while the blue areas correspond to the neural network's forecasted extent.

At the 1-month lead time forecast (Fig. 9), the CTL model exhibits a relatively strong ability to predict the geographic extent of moderate drought across most subregions. The model's predictions align closely with observed drought areas, especially in subregions R6, and R7, where the forecasted and observed drought extent show remarkable consistency. In R7, for example, the model successfully captures both the timing and extent of the significant drought events between 2008 and 2009, as well as those in 2015–2016 and 2019–2020.

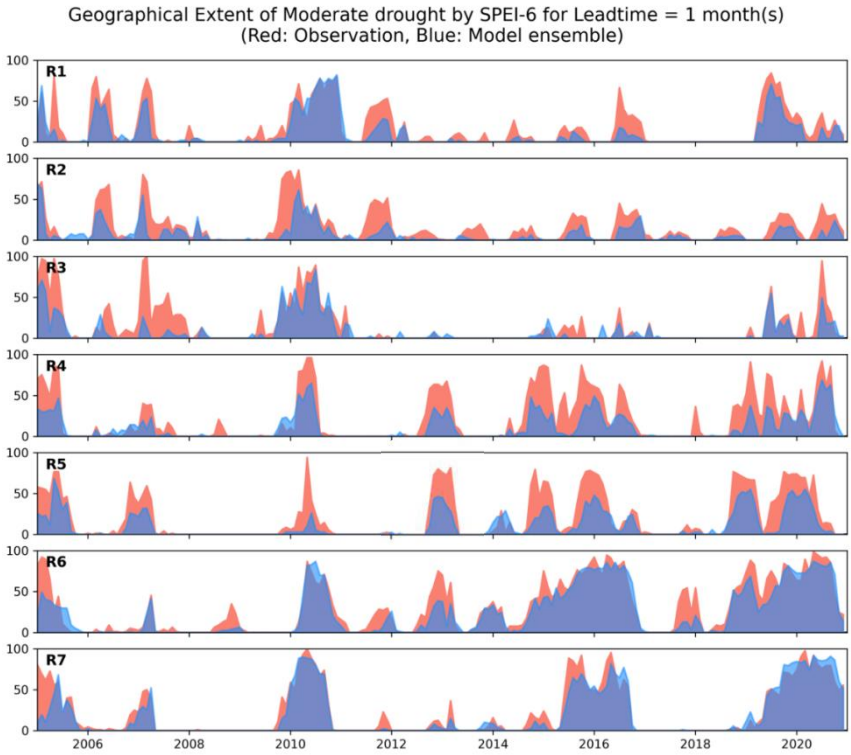

Figure 9. Geographical extent of Moderate drought by SPEI-6 fore 1-month lead time. Red areas denote observed extent, while blue areas denote CTL predicted extent

However, the underestimation of drought areas is more pronounced over subregions R1–R5. The peaks of drought extent in these periods are well-represented. With the complex topography and varied climate patterns of R4-5 (Van Khiem et al., 2014), the model manages to simulate the spatial distribution of drought events with some

underestimation, particularly during 2010 and 2015–2017 (30% difference). However, the overall pattern is captured reasonably well. During the 2015 drought at R4, the model predicted a maximum extent of 5%, whereas the observed extent was 50%, reflecting an underestimation of 45%. The close correspondence suggests that the neural network can incorporate the necessary parameters to predict droughts even in regions with diverse climate influences. While the model is generally reliable, it may struggle with certain local factors or extreme events. These minor deviations, though infrequent, highlight the need for further refinement in the ANN's ability to capture the full range of drought-driving mechanisms.

As the forecast lead time extends to 5 months, the model's performance in predicting the geographical extent of moderate drought varies among subregions (Fig. 10). In general, the fluctuations of geographical extent at 5-month lead time are smoothed out; the model appears to slightly lag the observed trends, especially during rapid changes from wet to dry conditions. A decline is particularly evident in subregions R1-2, R6 and R7. The underestimation is more pronounced in these subregions, and the neural network fails to capture several drought areas. The model significantly underestimates drought extent during significant events, such as in 2010, where the observed R2 extent reached 90%, but the model predicted only 40%.

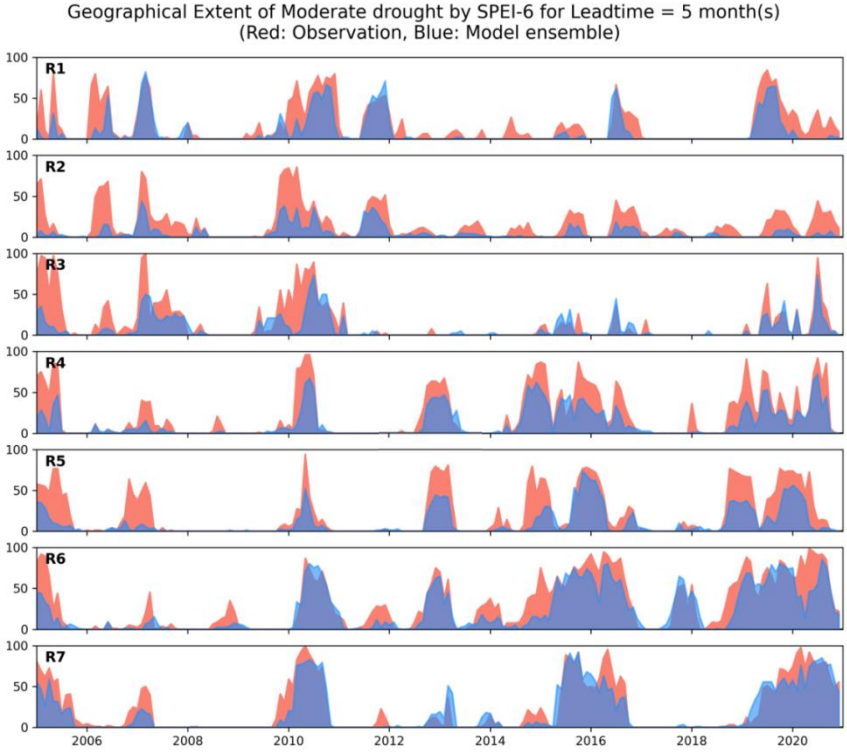

Figure 10. Geographical extent of Moderate drought by SPEI-6 fore 5-month lead time. Red areas denote observed extent, while blue areas denote CTL's predicted extent

In contrast, R3-R5 presents a mixed performance at the 5-month lead time. While the model still underestimates drought extent in some cases, the discrepancies are less pronounced or even better than the 1-month lead time. For example, the predicted drought

extent better aligns with observation during 2015 in R4 (a peak of 50%) and 2016 in R5 (a peak of 75%).

4. Concluding remarks

In this study, we constructed a new integration of a hybrid model in two distinct experiments to analyze the sensitivity of drought forecast over Vietnam using drought index SPEI on a 6-month scale. The hybrid model involves several steps, prominently featuring bias correction of precipitation and temperature data from regional climate models, clWRF, and RegCM4. Differences in the performance of the two dynamical RCMs indeed have the potential to impact the skill of both bias-corrected methods, such as Cli, ANN, and MLR, as variations in downscaled inputs could affect the accuracy of the drought forecast. The corrected outputs are then used to calculate SPEI-6, feeding into a multi-model ensemble strategy designated to reduce the uncertainties of standalone models. We developed two experiments in this: a feedforward and complex neural network architecture (ANN2), namely CTL, and an ensemble mean, ENS. These methodologies demonstrate the application of hybrid models in improving the reliability of drought forecasts.

Based on the prediction skills verified, it is plausible that the results are influenced by how well the model captures the relationship between monthly rainfall and, thus, the SPEI-6 index. Differences in rainfall distribution and intensity could lead to variations in the SPEI-6 response, affecting the overall predictability of drought events. The categorical verification metrics depicted excellent results, highlighting the performance of CTL over ENS. This distinction underscores the potential of neural network models in enhancing drought prediction accuracy compared to ensemble models in specific scenarios.

The comparison in different time scales highlights that the CTL's predictive skill of drought index SPEI-6 decreases as the lead times extend. At the 1-month lead time, the model more accurately captures both the timing and amplitude of the SPEI-6 across most subregions. However, as the lead time increases to 5 months, the model shows more significant discrepancies, particularly in the amplitude of extreme droughts. Besides, the quantitative analysis indicates that the model generally follows the observed data trends, suggesting its robustness in reflecting typical drought conditions even at longer lead times. This outcome highlights challenges in long-term drought forecasting under varying regional and climatic conditions.

The analysis of the geographic extent of moderate droughts reveals that while the CTL model performs well in short-term forecasting, its accuracy diminishes with longer lead times. This makes the neural network valuable for early warning systems and immediate drought response planning. The notable decline in accuracy at longer lead times, particularly at subregions with complex climate patterns, such as R5, highlights the need for model enhancements.

Although the CTL model demonstrates certain advantages when evaluated using corresponding multilayer perceptron architecture, there is no universal method for determining which type of architecture and training approach is most suitable for forecasting objectives. This study primarily highlights the potential benefits of CTL under specific parameter settings, yet selecting optimal ANN architectures remains an open challenge. The findings suggest that while CTL shows promise, the broader question of how to best design and train neural networks for drought forecasting still requires further exploration and refinement.

Future improvements could focus on better integrating these signals, enhancing the model's sensitivity to local climate factors,

and refining its representation of drought-driving mechanisms. On the one hand, expanding the model inputs to include more climate data affecting drought conditions, such as soil moisture, could improve the model's long-term forecasting capabilities. Additionally, enhancing hybrid models, combining neural networks with other advanced statistical or dynamical models, such as Adaptive Neuro-Fuzzy Inference System (ANFIS), Support Vector Machine (SVM), or Long Short-Term Memory (LSTM) networks, could strengthen drought forecasting performance in a nonlinear relationship.

Acknowledgments

This research was funded by Vietnam National University, Hanoi (VNU), under Grant Number QG.22.81.

Data availability statement

The datasets used in this manuscript are downloaded from the following websites: VnGP: http://danida.vnu.edu.vn/cpis/en/content/gridded-precipitation-data-of-vietnam.html; NCEP CFSv2: https://rda.ucar.edu/datasets/ds094.0. These are available online and open resources.

References

Adnan R.M., et al., 2021. Improving drought modeling using hybrid random vector functional link methods. Water, 13(23), 3379.

AghaKouchak A., et al., 2022. Status and prospects for drought forecasting: opportunities in artificial intelligence and hybrid physical-statistical forecasting. Philosophical Transactions of the Royal Society A: Mathematical, Physical and Engineering Sciences, 380.

Ali Z., et al., 2017. Forecasting Drought Using Multilayer Perceptron Artificial Neural Network Model. Advances in Meteorology. https://doi.org/10.1155/2017/5681308.

Alley R.B., Emanuel K.A., Zhang F., 2019. Advances in weather prediction. Science, 363(6425), 342–344.

ASCE, 2000. Artificial Neural Networks in Hydrology. I: Preliminary Concepts. Journal of Hydrologic Engineering, 5(2), 115–123.

Becker E., den Dool H.v., Zhang Q., 2014. Predictability and Forecast Skill in NMME. Journal of Climate, 27(15), 5891–5906.

Beguería S., Vicente Serrano S.M., Reig-Gracia F., Latorre Garcés B., 2014. Standardized precipitation evapotranspiration index (SPEI) revisited: parameter fitting, evapotranspiration models, tools, datasets and drought monitoring. International Journal of Climatology, 34, 3001–3023.

Belayneh A., Adamowski J., Khalil B., Ozga-Zielinski B., 2014. Long-term SPI drought forecasting in the Awash River Basin in Ethiopia using wavelet neural network and wavelet support vector regression models. Journal of Hydrology, 508, 418–429.

Dai A., 2011. Drought under global warming: a review. WIREs Climate Change, 2(1), 45–65.

Deo R.C., Şahin M., 2015. Application of the Artificial Neural Network model for prediction of monthly Standardized Precipitation and Evapotranspiration Index using hydrometeorological parameters and climate indices in eastern Australia. Atmospheric Research, 161–162, 65–81.

Guttman N.B., 1999. Accepting the Standardized Precipitation Index: A calculation algorithm. JAWRA Journal of the American Water Resources Association, 35(2), 311–322.

Habeeb R., et al., 2023. Modified Standardized Precipitation Evapotranspiration Index: spatiotemporal analysis of drought. Geomatics, Natural Hazards and Risk, 14(1), 2195532.

Hao Z., Singh V.P., Xia Y., 2018. Seasonal Drought Prediction: Advances, Challenges, and Future Prospects. Reviews of Geophysics, 56(1), 108–141.

Heaton J., 2008. Introduction to Neural Networks for Java, Heaton Research Inc., ISBN: 978-1-60439-00-7, 380p.

Heim Jr R.R., 2002. A review of twentieth-century drought indices used in the United States. Bulletin of the American Meteorological Society, 83(8), 1149–1166.

Hornik K., Stinchcombe M., White H., 1990. Universal approximation of an unknown mapping and its derivatives using multilayer feedforward networks. Neural Networks, 3(5), 551–560.

Kim T.-W., Valdés Juan B., 2003. Nonlinear Model for Drought Forecasting Based on a Conjunction of Wavelet Transforms and Neural Networks. Journal of Hydrologic Engineering, 8(6), 319–328.

Kůrková V., 1992. Kolmogorov's theorem and multilayer neural networks. Neural networks, 5(3), 501–506.

Le J.A., El-Askary H.M., Allali M., Struppa D.C., 2017. Application of recurrent neural networks for drought projections in California. Atmospheric Research, 188, 100–106.

Le P.V.V., Phan-Van T., Mai K.V., Tran D.Q., 2019. Space-time variability of drought over Vietnam. International Journal of Climatology, 39(14), 5437–5451.

Lorenz E.N., 1963. Deterministic nonperiodic flow. Journal of the Atmospheric Sciences, 20, 130–141.

Madadgar S., Moradkhani H., 2014. Spatio-temporal drought forecasting within Bayesian networks. Journal of Hydrology, 512, 134–146.

McCulloch W.S., Pitts W., 1943. A logical calculus of the ideas immanent in nervous activity. The bulletin of mathematical biophysics, 5(4), 115–133.

Mckee T.B., Doesken N.J., Kleist J.R., 1993. The relationship of drought frequency and duration to time scales. 8th Conference on Applied Climatology, Anaheim, 179–184.

McKee T.B., Doesken N.J., Kleist J., American Meteorological S., 1995. Drought Monitoring with Multiple Time Scales, 9th Conference, Applied climatology. The Society, Dallas, TX, 233–236.

Mezard M., Nadal J.-P., 1999. Learning in feedforward layered networks: The tiling algorithm. Journal of Physics A: Mathematical and General, 22, 2191.

Mishra A., Desai V., 2006. Drought forecasting using feedforward recursive neural network. Ecological Modelling, 198, 127–138.

Mishra A.K., Desai V.R., 2005. Drought forecasting using stochastic models. Stochastic Environmental Research and Risk Assessment, 19(5), 326–339.

Mishra A.K., Singh V.P., 2011. Drought modeling - A review. Journal of Hydrology, 403(1), 157–175.

Morid S., Smakhtin V., Bagherzadeh K., 2007. Drought forecasting using artificial neural networks and time series of drought indices. International Journal of Climatology, 27(15), 2103–2111.

Nguyen D.Q., Renwick J., McGregor J., 2014. Variations of surface temperature and rainfall in Vietnam from 1971 to 2010. International Journal of Climatology, 34(1), 249–264.

Nguyen-Xuan T., et al., 2016. The Vietnam Gridded Precipitation (VnGP) Dataset: Construction and Validation. SOLA, 12, 291–296.

Phan V., et al., 2014. Observed climate variations and change in Vietnam. Mckee T.B., Doesken N.J., Kleist J.R., 1993. The relationship of drought frequency and duration to time scales. In EWATEC-COAST: Technologies for Environmental and Water Protection of Coastal Zones in Vietnam. Contributions to 4th International Conference for Environment and Natural Resources, ICENR 2014. Cuvillier, Göttingen, Germany. ISSN: 2363-7218. ISBN: 978-3-95404-852-6.

Phan V.-T., Ngo-Duc T., 2009. Seasonal and interannual variations of surface climate elements over Vietnam. Climate Research, 40(1), 49–60.

Phan-Van T., et al., 2018. Evaluation of the NCEP Climate Forecast System and Its Downscaling for Seasonal Rainfall Prediction over Vietnam. Weather and Forecasting, 33(3), 615–640.

Phan-Van T., et al., 2022. Drought over Southeast Asia and Its Association with Large-Scale Drivers. Journal of Climate, 35(15), 4959–4978.

Phan-Van T., Ngo-Duc T., Ho-Hagemann H., 2009. Seasonal and interannual variations of surface climate elements over Vietnam. Climate Research, 40, 49–60.

Rayhan M., Afroz R., 2024. Evaluating climate models to analyze drought conditions in the western region of Bangladesh. Progress in Disaster Science, 23, 100356.

Saha S., et al., 2014. The NCEP Climate Forecast System Version 2. Journal of Climate, 27(6), 2185–2208.

Santos C., Morais B., Silva G., 2009. Drought forecast using Artificial Neural Network for three hydrological zones in San Francisco river basin. IAHS Publication, 333, 302–312.

Sardar V.S., Y. K,M., Chaudhari S.S., Ghosh P., 2021. Convolution Neural Network-based Agriculture Drought Prediction using Satellite Images, 2021 IEEE Mysore Sub Section International Conference (MysuruCon), 601–607.

Schmidt C., Overhoff H., 2022. Impact of PCA-based preprocessing and different CNN structures on deformable registration of sonograms, WSCG 2022 Proceedings: Computer Science Research Notes, ISSN 2464–4617, 181–188.

Shobha P., et al., 2023. Drought Prediction Using Recurrent Neural Networks and Long Short-Term Memory Model. Sentiment Analysis and Deep Learning. Springer Nature Singapore, Singapore, 97–103.

Spinoni J., et al., 2020. Future Global Meteorological Drought Hot Spots: A Study Based on CORDEX Data. Journal of Climate, 33(9), 3635–3661.

Steinemann A., Hayes M.J., Cavalcanti L.F.N., 2005. Drought Indicators and Triggers, 71–92.

Sudheer K.P., Gosain A.K., Ramasastri K.S., 2003. Estimating Actual Evapotranspiration from Limited Climatic Data Using Neural Computing Technique. Journal of Irrigation and Drainage Engineering, 129(3), 214–218.

Tan C., Yang J., Li M., 2015. Temporal-spatial variation of drought indicated by SPI and SPEI in Ningxia Hui Autonomous Region, China. Atmosphere, 6(10), 1399–1421.

Thilakarathne M., Sridhar V., 2017. Characterization of future drought conditions in the Lower Mekong River Basin. Weather and Climate Extremes, 17, 47–58.

Thornthwaite C.W., 1948. An Approach toward a Rational Classification of Climate. Geographical Review, 38(1), 55–94.

Tran-Anh Q., Ngo-Duc T., Espagne E., Trinh-Tuan L., 2022. A high-resolution projected climate dataset for Vietnam: Construction and preliminary application in assessing future change. Journal of Water and Climate Change, 13(9), 3379–3399.

Trenberth K.E., et al., 2014. Global warming and changes in drought. Nature Climate Change, 4(1), 17–22.

Van Khiem M., Redmond G., McSweeney C., Thuc T., 2014. Evaluation of dynamically downscaled ensemble climate simulations for Vietnam. International Journal of Climatology, 34(7), 2450–2463.

Vicente-Serrano S.M., Beguería S., López-Moreno J.I., 2010. A multiscalar drought index sensitive to global warming: the standardized precipitation evapotranspiration index. Journal of climate, 23(7), 1696–1718.

Vu H., Ngo-Duc T., Phan-Van T., 2013. Evolution of meteorological drought characteristics in Vietnam during the 1961-2007 period. Theoretical and Applied Climatology, 118.

Vu M.T., Raghavan S.V., Pham D.M., Liong S.-Y., 2015. Investigating drought over the Central Highland, Vietnam, using regional climate models. Journal of Hydrology, 526, 265–273.

Wang D., et al., 2018. A hybrid wavelet de-noising and Rank-Set Pair Analysis approach for forecasting hydro-meteorological time series. Environmental Research, 160, 269–281.

Watanabe M., et al., 2010. Improved climate simulation by MIROC5: mean states, variability, and climate sensitivity. Journal of Climate, 23(23), 6312–6335.

Wilhite D., Buchanan-Smith M., 2005. Drought as hazard: Understanding the natural and social context, 3–29.

WMO, 2006. Drought monitoring and early warning : concepts, progress, and future challenges. WMO (Series); no. 1006. World Meteorological Organization, Geneva, Switzerland.

Woldeyohannes D.-Y., Vaheddoost B., Al-Weshah D.-R., 2019. Drought indices and indicators revisited. Arabian Journal of Geosciences, 12, 1–12.

Wu Z., Yin H., He H., Li Y., 2022. Dynamic-LSTM hybrid models to improve seasonal drought predictions over China. Journal of Hydrology, 615, 128706.

Yihdego Y., Vaheddoost B., Al-Weshah R.A., 2019. Drought indices and indicators revisited. Arabian Journal of Geosciences, 12(3), 69.

Zarei A.R., Moghimi M.M., 2019. Modified version for SPEI to evaluate and modeling the agricultural drought severity. International Journal of Biometeorology, 63(7), 911–925.

Zargar A., Sadiq R., Naser B., 2011. A review of drought indices. Environmental Reviews, 19, 333–349.

Zhang Q., et al., 2024. Multivariate time series convolutional neural networks for long-term agricultural drought prediction under global warming. Agricultural Water Management, 292, 108683.

Zhang Y., Li T., Wang B., Wu G., 2002. Onset of the summer monsoon over the Indochina Peninsula: Climatology and interannual variations. Journal of Climate, 15(22), 3206–3221.

Zhang Z., Chao B.F., Chen J., Wilson C.R., 2015. Terrestrial water storage anomalies of Yangtze River Basin droughts observed by GRACE and connections with ENSO. Global and Planetary Change, 126, 35–45.